JHEP PROCEEDINGS

International Europhysics Conference on HEP

Recent Results from the CMB

Ken Ganga* **& E. Hivon**

Infrared Processing and Analysis Center
Mail Code 100-22; California Institute of Technology
Pasadena, CA 91125; USA
E-mail: kmg@ipac.caltech.edu

P.A.R. Ade & P.D. Mauskopf – Cardiff University, Wales, UK

J.J. Bock – Jet Propulsion Laboratory, CA, USA

J.R. Bond, C.R. Contaldi, D. Pogosyan & S. Prunet – CITA, Toronto, Canada

J. Borrill – NERSC, LBNL, Berkeley, CA, USA

A. Boscaleri & E. Pascale – IROE-CNR, Firenze, Italy

K. Coble, P. Farese, T. Montroy & J.E. Ruhl – Physics Dept., UCSB, CA, USA

B.P. Crill, V.V. Hristov, W.C. Jones, A.E. Lange, & P. Mason – Caltech, Pasadena, CA, USA

P. de Bernardis, M. Giacometti, A. Iacoangeli, L. Martinis, S. Masi, F. Piacentini, F. Pongetti, F. Scaramuzzi – Dipartimento di Fisica, Universita' La Sapienza, Roma, Italy

A.H. Jaffe – Department of Astronomy, Berkeley, CA, USA

A. Melchiorri – University of Oxford, Oxford, UK

C.B. Netterfield – Depts. of Physics and Astronomy, University of Toronto, Canada

G. Romeo – Istituto Nazionale di Geofisica, Roma, Italy

Abstract: We review recent strides in understanding the universe through measurements of anisotropies in the cosmic microwave background radiation. Particular emphasis is given to the BOOMERanG experiment and results.

1. Introduction

The cosmic microwave background (CMB) radiation is now generally understood to be remnant radiation from the early history of the universe – approximately 300000 years

*Speaker.

after the big bang. First detected and recognized as such in 1965 by Penzias and Wilson [1] and Dicke et al. [2], to first order it manifests itself as radiation coming towards us with uniform intensity in all directions (see Figure 1). The FIRAS instrument on board the COBE satellite has made the most precise measurements to date of the spectrum of the CMB [3], confirming its blackbody nature, as we would expect from such a thermal source.

Much of the value derived from studying the CMB, however, is realized by digging deeper and examining the spatial anisotropies in the CMB. If we remove an offset from a map of the CMB sky, which most anisotropy experiments such as COBE/DMR do automatically, we are essentially left with the so-called CMB dipole, as shown in Figure 2. This dipole, roughly three orders of magnitude smaller than the CMB monopole, is not cosmological in origin, but rather reflects the fact that the Sun, and thus the Earth and our experiments, are moving with respect to the frame of reference of the CMB. Photons from the CMB impinging upon us from the direction opposite our motion are doppler blue-shifted, while those from the other direction are red-shifted. This too can be effectively removed, yielding an underlying pattern roughly two orders of magnitude smaller still than the dipole anisotropy (Figure 3).

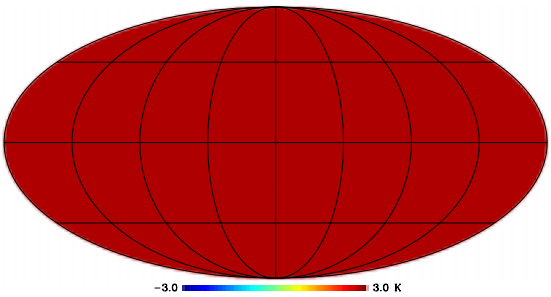

Figure 1: A representation of the large CMB monopole, which dominates emission in this frequency range. This plot is essentially the same as the next, from COBE/DMR at 53 GHz, but has an additional 2.7 K offset added. These data were obtained from [4].

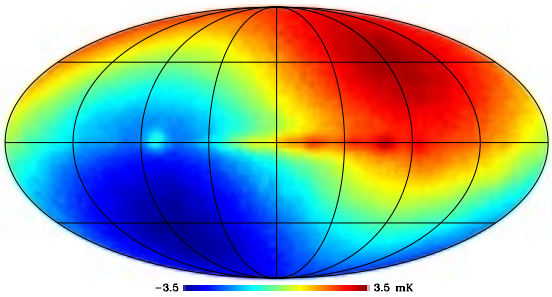

Figure 2: The dipole emission due to the sun's motion through the CMB, which is the next most dominant effect after the monopole. These data were obtained from [4].

Some of these underlying fluctuations are cosmological, but some are decidedly not. The wide red band in the center of Figure 3 is, for example, radiation from our own Galaxy. One of the major considerations in both the design and data reduction of CMB anisotropy experiments is to minimize the effects of such foreground emissions through appropriate experimental design and data reduction which exploits the spatial and spectral differences between the CMB and these foregrounds.

To understand how the fluctuations in CMB anisotropy maps can help us understand our cosmogony, consider that in the standard cosmology, after baryons are created, the universe can be seen as a hot, dense soup of ionized baryons, photons, and perhaps other types of matter and energy. The matter at a particular scale begins to collapse after time.

After even more time, as over-densities grow to a certain point, photon pressure will reverse this gravitational collapse, and in the absence of other factors, the density on this particular scale would oscillate between over- and under-dense.

The universe, however, is expanding. As it does so, it, and the photons within it, are cooling. When it reaches the point where the CMB photons no longer have the energy to ionize hydrogen, the protons and electrons combine once and for all into hydrogen. At this point the photons no longer interact effectively with the baryons, and they thus travel to us with only sporadic interaction with matter, thus providing us with a snapshot of the early universe at the so-called last scattering surface or epoch of recombination.

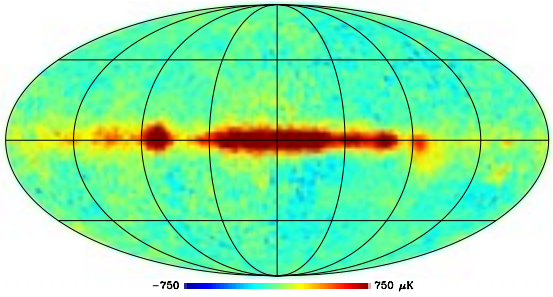

Figure 3: The residuals after the dipole emission is removed from the COBE/DMR 53 GHz map. The strong emission in the center of the plot represents Galactic emission, but the variations above and below this are dominated by instrumental noise and anisotropies in the CMB. These data were obtained from [4].

Since different scales will oscillate at different rates, with smaller regions collapsing sooner than larger ones, if this recombination can be considered to be instantaneous, we will see that different scales will have compressed different amounts. Starting at some small scale, say one that has had time to compress, rarify, and then compress again, we will see a peak in the power spectrum of the anisotropies. As we move to larger scales, we will get to an angular scale which has only had time to compress and then rarify, Finally, continuing to move to larger scales, we come to regions of such a scale that they have only had time to compress before the universe recombines. Regions larger than this have not had time to compress.

Now, given a certain sized structure at recombination, its angular size as we view it will be determined by the geometry of the universe – its angular size will be smaller in an open universe than in a flat one (see Figure 4 for a cartoon demonstration of this geometrical effect).

This and further concepts are best understood by resorting to a spherical power spectrum of anisotropies, as shown in Figure 5. The black line in Figure 5 is a "reasonable" model – it has $\Omega_b = 0.03858$, $\Omega_c = 0.25$ and $\Lambda = 0.71142$ (implying that $\Omega_{\rm total} = 1$). H_0 was chosen to be 72 km/s/Mpc. The red line in the same figure has exactly the same parameters, except that $\Lambda = 0$, giving us an open universe with the same matter content as the first. The first peak defines a characteristic scale at the surface of last scattering, and we can see that this is at higher

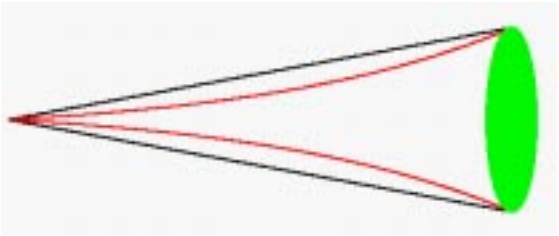

Figure 4: A cartoon to demonstrate the geometrical effect which causes structures of a given size at the epoch of recombination to appear smaller in open universes than in flat ones.

multipoles (= smaller angular scales) for the open (red) model than for the flat (black) model. The series of peaks can be seen in all the spectra.

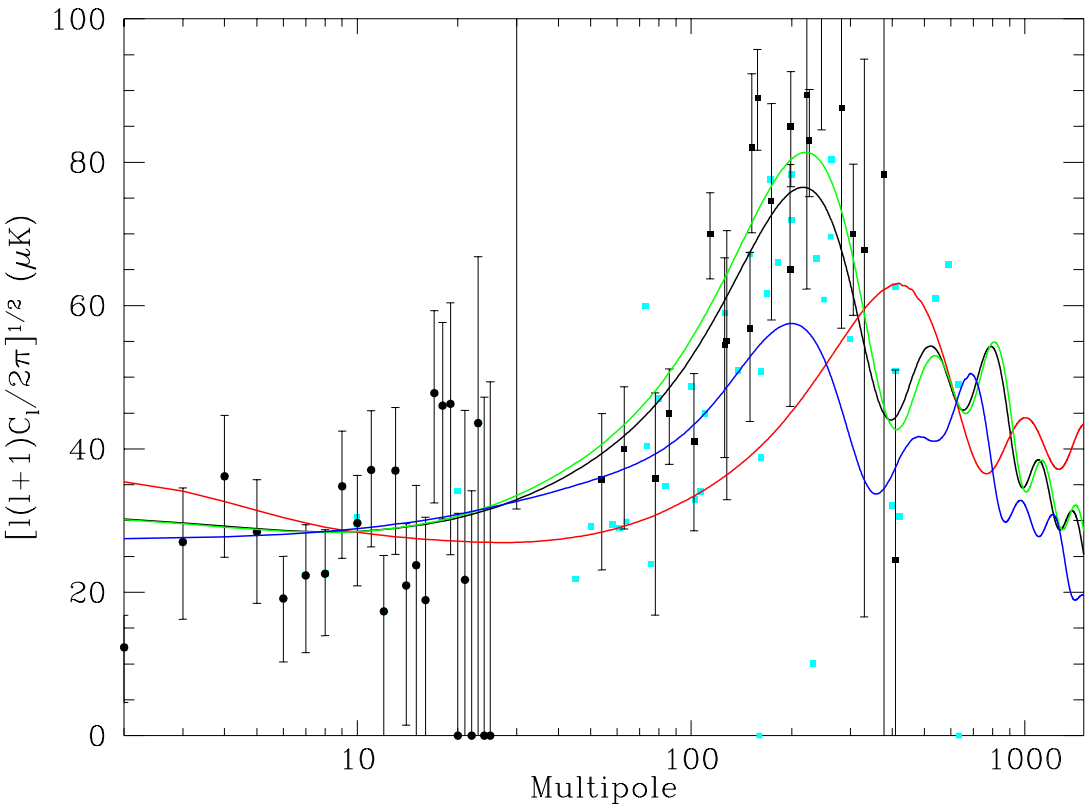

Figure 5: The state of CMB anisotropies at the end of the last millennium. The data points represent decades of CMB anisotropy measurements. To make the plot readable, most of the points are plotted in light blue without error bars. The black points on the left of the plot (at low multipoles) come from COBE/DMR. The black points around the first peak are from a set of Princeton/Penn experiments. The theoretical spectra shown are: Black line – Ω_b=0.03858, Ω_c=0.25, Ω_v=0.71142; Red line – Ω_b=0.03858, Ω_c=0.25, Ω_v=0.0; Green line – Ω_b=0.05, Ω_c=0.23858, Ω_v=0.0; Blue line – Ω_b=0.03858, Ω_c=0.96142, Ω_v=0.0. In all cases, h=0.72. The experimental data were taken from a compilation by Knox [5]. The spectra were created with the CMBFast software [6].

The angular resolution of COBE/DMR was roughly seven degrees, shown as the data points on the left of Figure 5. The scale of the horizon when the CMB last scattered is, however, of order a degree. Before the recent measurements by BOOMERanG, DASI and MAXIMA, "getting the first peak" was one of the primary goals in the CMB field, precisely to make these finer angular scale measurements and to resolve the intermediate and small scale structure in the CMB. The cloud of light blue points in Figure 5 attests to the effort that has been put into this, and the difficulty in nailing it down precisely. We note, however, that a series of experiments from Princeton and Penn had essentially done this [7, 8, 9], though with lower signal-to-noise than has been obtained recently.

The further understanding that can be gained by these measurements is shown by considering the baryon fraction. The green spectrum in Figure 5 is similar to the black in that it has the same total density, Hubble's constant and cosmological constant, but differs in that it has a higher baryon to cold dark matter fraction. Note that the *difference* in the heights of the first two peaks is changed by changing the baryon content. This can be understood by noting that while all matter (baryons and the cold dark matter included) collapses gravitationally, only the baryons are subject to the photon pressure. This thus causes an asymmetry in the even and odd numbered peak heights, and gives us a convenient way to pin down the baryon content of the universe. This will be shown with the BOOMERanG data below.

2. BOOMERanG

BOOMERanG (Balloon Observations Of Millimetric Extragalactic Radiation and Geomagnetics) is a long-duration, balloon-borne experiment designed to measure anisotropies in the cosmic microwave background on angular scales from degrees to arc-minutes. It was conceived by two co-PIs, Paolo de Bernardis from La Sapienza, Rome and Andrew Lange from Caltech in Pasadena, CA. They lead the international collaboration along with Silvia Masi, also of La Sapienza, John Ruhl of Santa Barbara, Phil Mauskopf of Cardiff and Barth Netterfield of Toronto.

BOOMERanG has flown twice – once for a single night in 1997 from North America as a technical verification flight [10], and once from McMurdo Station, Antarctica in a flight that started December 29, 1998 and gathered over 250 hours of data from an altitude of roughly 40 km. During the 1998-9 flight, on which we will concentrate here, the balloon remained afloat for over ten days and circumnavigated the South Pole roughly along the 79° south parallel (note that there is no guidance system; the path was determined by polar winds). The package was dropped after 10.5 days and landed within 50 km of where it took off, making recovery of the instrument and future flights possible (See Figure 6).

Observations were made simultaneously in 16 different channels covering 4 different frequency bands at 90, 150, 240 and 400 GHz. The mirror is a 1.2 m, off-axis parabolic. To scan in azimuth, the entire gondola moves, while to steer in elevation an inner frame with both the receiver and the optics can be moved. During observations, the telescope is fixed at a particular elevation (which is adjustable). Because observations are made from near the south pole in summer, BOOMERanG could observe regions 24 hours a day, without them setting and rising. It is a happy coincidence (which was known and intentionally exploited) that the south Galactic pole, a region of low foreground contamination, is one of those regions away from the sun and visible 24 hours a day from the south pole in the summer.

Roughly four percent of the sky was observed for primary CMB work. Figure 7 shows the location of the observations relative to a COBE/DMR map (in equatorial coordinates), while Figure 8 shows a 150 GHz map (upper panel), along with a map of the integration time (lower panel). In the upper panel of Figure 8, the roughly square region marked in the center of the plot shows the region used for the first analysis of de Bernardis et al. [13].

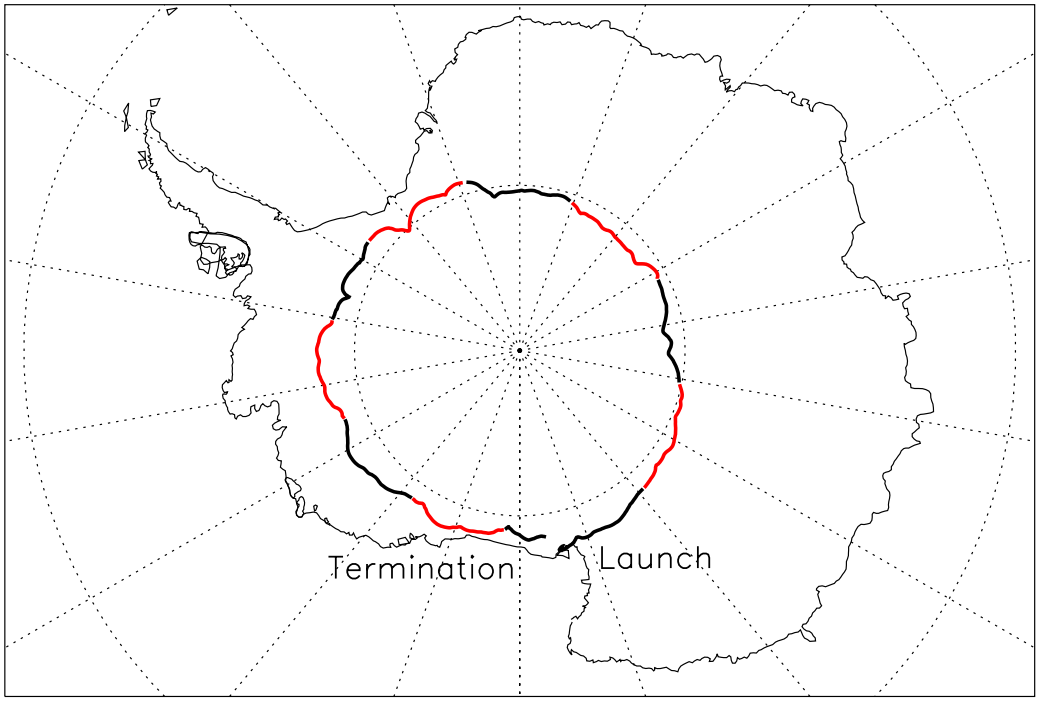

Figure 6: The path of the LDB flight of BOOMERanG. Alternate days are shown successively in black and red. See [12].

The larger ellipse marks the sky coverage used in the more recent analysis of Netterfield et al. [14]. The three small circles mark the locations of radio sources in the maps.

Because experiments such as BOOMERanG have so-called "1/f" noise, maps cannot be made and well-characterized in terms of the noise properties by simply "binning" the data, as individual samples are not uncorrelated. The BOOMERanG maps are made, accounting for this, with an iterative Jacobi method which gives us both a map as well as the non-trivial power spectrum for the noise of the measurements [30]. In Figures 9, 10, 11 and 12, we show maps obtained at each frequency.

A few things should be noted about these maps. Our primary CMB channel was 150 GHz. Lines of constant Galactic latitude, b, are marked towards the right-hand sides of the plots at $b = -5$ degrees and $b = -15$ degrees; thus, the Galactic plane would be off the plot towards the right of the graphic. In the higher frequency channels, Galactic emission can be seen beginning to show up as we get closer to the plane.

In the higher frequency channels, regions of low emission values can be seen right next to the emission near the Galactic plane. This is, in fact, simply an artifact of the high-pass filtering which is done directly on the time-stream data in order to mitigate the effects of the 1/f noise mentioned above. This effect is accounted for by 1) using regions away from areas thus affected and 2) accounting for the effect mathematically when we calculate the power spectra from the maps.

As mentioned above, one of the first orders of business is for us to confirm that Galactic

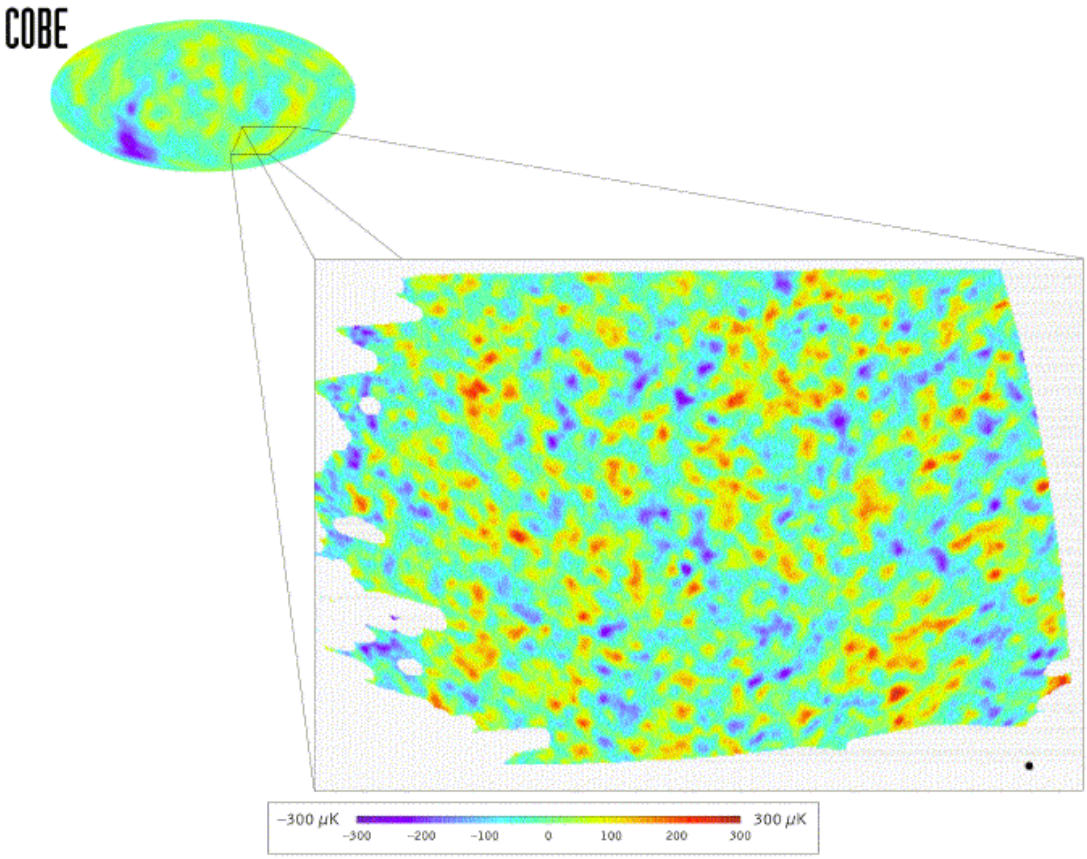

Figure 7: The BOOMERanG coverage compared to that of COBE/DMR. Note that the differences between this figure and Figure 3 are a result of binning in different coordinate systems, Galactic emission removal, and smoothing.

emission has not significantly contaminated the CMB measurements. For this, we use the channels other than our prime CMB channels (150 GHz) as a check. One visual demonstration of this is provided by simply subtracting the map made at 240 GHz from the map at 150 GHz, as is shown in Figure 13. This qualitatively shows, since the residuals are much smaller than the signals in either of the two channels separately, that foreground emission is not much of an issue. If dust, for example, were a problem, this map would resemble the 400 GHz map (Figure 12) much more strongly, as the 400 GHz maps is dominated by Galactic dust emission. There does seem to be some low level dust emission; Masi et al. [15], however, have shown that it is not significant compared to the CMB emission at 150 GHz.

With the CMB map in hand, we can now calculate its power spectrum. This is the most computationally challenging aspect of the data reduction. Essentially, we are trying to solve for the power spectrum, C_l, which maximizes the likelihood, defined by

$$\mathcal{L} = \frac{1}{\sqrt{(2\pi)^n |\mathbf{M}|}} e^{\mathbf{p}^T \mathbf{M}^{-1} \mathbf{p}}, \tag{2.1}$$

where $\mathbf{p}$ is a vector of map pixel values and $\mathbf{M}$ is the pixel-pixel covariance matrix. $\mathbf{M}$ can

be further reduced to

$$\mathbf{M} = \mathbf{S} + \mathbf{N}, \tag{2.2}$$

where **S** represents the correlations intrinsic to the CMB anisotropies and **N** represents the noise correlations that arise from the experiment. Finally, we can relate the sky correlation matrix, **S**, to the power spectrum, C_l, which is what we're interested in, via the relation

$$S_{i,j} = \sum_l \frac{2l+1}{4\pi} C_l B_l P_l \left(\cos\left(\theta_{i,j}\right)\right). \tag{2.3}$$

Here, l is a multipole moment, i and j are pixel indices, B_l is the square of the Legendre transform of be beam, and $P_l\left(\cos\left(\theta_{i,j}\right)\right)$ is the Legendre polynomial of order l evaluated at the cosine of the angle between pixels i and j.

The first complication with this system is that it is non-linear; i.e., the object we are looking for, C_l, does not depend linearly on what we know, **s**. This, however, is not the largest hurdle; the sheer size of the system is.

Sometimes one can assume that the noise is uncorrelated from pixel to pixel, which allows one to ignore all but the diagonal elements of the noise matrix, **N**, which are then simply equal to $\sigma^2_{\rm pixel}$. Unfortunately, the 1/f noise, as well as time-line filtering and other experimental effects such as atmospheric emission, make this a bad assumption for most CMB experiments. This means that we must deal with non-trivial matrices of order $n \times n$, where n is the number of pixels. In our case, n is roughly 60000 or more, making the system difficult to deal with.

We have addressed this in two way: 1) brute force and 2) using monte carlos. In the former case, we solve the system using the US National Energy Research Scientific Computing Center IBM SP, one of the 5 largest computing facilities in the world [16] using the MADCAP code [17]. This yields optimal results, but is too resource-consuming to do too often (for example, during testing, debugging, checking, etc.). In the latter case, a set of judiciously chosen monte carlos allows us to get a non-optimal solution which is never-the-less competitive with the optimal results, but which requires a fraction of the resources [18]. The two methods give consistent results. The results from the latter are shown in Figure 14. Note that the Planck experiment will have millions of pixels, making the brute force approach that much more difficult.

It must also be emphasized that while we have focussed here on BOOMERanG results, two other experiments, DASI [19, 21, 20] and MAXIMA [22], have also obtained comparably sensitive measurements of the power spectrum recently. The power spectra from these experiments are also shown in Figure 14, in magenta and light blue, respectively. The good agreement between three different experiments, each of which takes data differently and reduces this data differently, is a powerful check that the results seen are not experimental systematics, misunderstood foreground emission, or simple data analysis mistakes.

3. Cosmology

With the power spectrum and its associated error matrix in hand, we can proceed to determining cosmological parameters. This is done by 1) creating a database of theoretical

power spectra for a wide range of "possible" cosmological parameters, 2) finding the chi-squared (or some similar statistic) and thus the likelihood that we would get our data set given each of the theoretical models and the noise, 3) apply a set of priors to get the probability of each of the models given our data, 4) marginalize over some variables to obtain lower dimensional probabilities for the parameters of interest and finally 5) extract values and limits for the parameters of interest.

So, to begin with, we create a database of theoretical power spectra like those in Figure 5. We have chosen to explore a 7-dimensional cosmological parameter space in the context of adiabatic inflationary models. In Lange et al. [28], we made models with

$$\begin{aligned}
\omega_c &= 0.03, 0.06, 0.12, 0.17, 0.22, 0.27, 0.33, 0.40, 0.55, 0.8, \\
\omega_b &= 0.003125, 0.00625, 0.0125, 0.0175, 0.020, \\
&\quad 0.025, 0.030, 0.035, 0.04, 0.05, 0.075, 0.10, 0.15, 0.2, \\
\Omega_\Lambda &= 0, 0.1, 0.2, 0.3, 0.4, 0.5, 0.6, 0.7, 0.8, 0.9, 1.0, 1.1, \\
\Omega_k &= 0.9, 0.7, 0.5, 0.3, 0.2, 0.15, 0.1, 0.05, 0, -0.05, -0.1, -0.15, -0.2, -0.3, -0.5, \\
n_s &= 1.5, 1.45, 1.4, 1.35, 1.3, 1.25, 1.2, 1.175, 1.15, 1.125, 1.1, 1.075, 1.05, \\
&\quad 1.025, 1.0, 0.975, 0.95, 0.925, 0.9, 0.875, 0.85, 0.825, 0.8, 0.775, \\
&\quad 0.75, 0.725, 0.7, 0.65, 0.6, 0.55, 0.5, \\
\tau_c &= 0, 0.025, 0.05, 0.075, 0.1, 0.15, 0.2, 0.3, 0.5.
\end{aligned}$$

Here, $\omega_x = \Omega_x h^2$, where x can be b for baryons, c for cold, dark matter, Λ for a cosmological constant, k for total curvature. In addition, there is an overall amplitude which we can conveniently vary continuously. This gives us a database of over seven million likelihoods of our data given the specified models. To this, we can also add parameters representing an overall calibration and our beam uncertainty, for example.

To convert these likelihoods to probabilities that a model is the one underlaying our data, we must assume certain priors. Note that even the simple fact that we cannot explore the infinite space of possibilities, and thus the fact that we set the priors to zero for models we think are *very* unlikely to zero, is in itself a prior. For all numbers quoted, a weak prior in which only models with $0.45 < h < 0.90$ is considered at a minimum. We then successively add more restrictive priors.

To this, we also add prior information about these models gleaned from measurements of large scale structure (LSS; [23]), and from recent measurements of type 1a supernovae (SN1a; [24, 25]). The "strong" h prior used is a Gaussian with a central value of 0.72 and ± 1 σ widths of 0.08, as implied from Hubble measurements. Finally, we also investigate the effects of assuming that the universe if flat.

For each prior, with this multi-dimensional hypersurface of probabilities in hand, we then marginalize over certain parameters in order to find our preferred values and limits for those remaining parameters. For example, by marginalizing over all parameters except $\Omega_{\rm matter}$ and Ω_Λ, we obtain the two-dimensional likelihoods for these parameters alone, as shown in Figure 15. This shows, in blue, that BOOMERanG has good discrimination power for the *total* energy density (i.e., $\Omega_m + \Omega_\Lambda$), but not much ability to discriminate

between different types of energy constituents. This is another reflection of the fact that one of the things BOOMERanG does best is determine the *position* of the first peak in Figure 14, which is in general a indication of the total energy density. However, by combining CMB measurements with those from other fields, for example measurements of type 1a supernovae as also shown in the figure [24, 25], much more robust limits on both the total energy density and that due to a cosmological constant can be derived, as is shown by the black line contours.

The same can be done for $\Omega_b h^2$ and n_s, as shown in Figure 16, or any other set of parameters. Figure 16 shows that the BOOMERanG determination of the scalar spectral index of perturbations is close to 1, consistent with inflationary predictions.

The measurement of $\Omega_b h^2$ is also consistent with that derived by Tytler et al. [27] using Big Bang Nucleosynthesis and measurements of light element abundances. This is a bit of a change from the values of $\Omega_b h^2$ first quoted by the BOOMERanG team; the differences are due primarily more data, and also to a better understanding of the pointing, a mistake in which can have the effect of changing the relative heights of the first and second peaks in the power spectrum.

Continuing in this same vein, for each parameter, we marginalize over all others to get one-dimensional probability curves. These are shown in Figure 17, for a variety of the priors used. The middle pane of the top panel, for example, indicates the difficulty BOOMERanG by itself has on setting limits on Λ, but how powerful the combination of BOOMERanG and other measurements can be.

From the one-dimensional curves we can get the favored values and error bars by finding the points where half of the probability curve is above and half is below, and find limits in similar fashion. The results are shown in Table 1. The results with our weak prior on the Hubble constant is shown in the top line, those with progressively stronger priors are shown in the successive three lines, and finally, similar results obtained by also assuming that $\Omega_{\rm total} = 1$ are show in the last three lines.

These are some of the most powerful measurements made to date in cosmology. Interpreting them should be made with care, however. We note that the method we use to marginalize over all but one parameter to set limits produces some non-intuitive results. For example, the sum of the most likely individual energy contributions does not sum to the most likely total. Taken as a whole, however, they constitute consistently powerful support for the inflationary cosmological scenario.

4. Conclusion

For many years, pundits have been predicting that studies of the anisotropies in the cosmic microwave background radiation would ultimately provide us with some of the most powerful measures of the universe we live in. With the recent measurements done by BOOMERanG, DASI and MAXIMA, decades of effort have finally made this hope a reality, giving us new insights into the matter content of the universe.

This effort, of course, is not done. The MAP satellite was launched in June of 2001 and is now making, we assume, even more sensitive maps of the CMB. If all works according

Priors	Ω_{tot}	n_s	$\Omega_b h^2$	$\Omega_{cdm} h^2$	Ω_Λ	Ω_m	Ω_b	h	Age
Weak only	$1.02^{0.06}_{0.06}$	$0.96^{0.10}_{0.09}$	$0.022^{0.004}_{0.003}$	$0.13^{0.05}_{0.05}$	$(0.51^{0.23}_{0.20})$	$(0.51^{0.20}_{0.20})$	$0.07^{0.03}_{0.03}$	$(0.56^{0.10}_{0.10})$	$15.2^{1.9}_{1.9}$
LSS	$1.02^{0.04}_{0.05}$	$0.97^{0.10}_{0.08}$	$0.022^{0.004}_{0.003}$	$0.13^{0.03}_{0.02}$	$0.55^{0.09}_{0.09}$	$0.49^{0.12}_{0.12}$	$0.07^{0.02}_{0.02}$	$0.56^{0.09}_{0.09}$	$15.0^{1.3}_{1.3}$
SN1a	$1.02^{0.07}_{0.05}$	$0.99^{0.11}_{0.10}$	$0.023^{0.004}_{0.004}$	$0.10^{0.04}_{0.04}$	$0.73^{0.07}_{0.10}$	$0.31^{0.06}_{0.06}$	$0.06^{0.03}_{0.03}$	$0.61^{0.09}_{0.09}$	$15.9^{2.5}_{2.5}$
LSS & SN1a	$0.99^{0.03}_{0.04}$	$1.03^{0.10}_{0.09}$	$0.023^{0.003}_{0.003}$	$0.14^{0.03}_{0.02}$	$0.65^{0.05}_{0.06}$	$0.34^{0.07}_{0.07}$	$0.05^{0.02}_{0.02}$	$0.67^{0.09}_{0.09}$	$13.7^{1.2}_{1.2}$
$h = 0.71 \pm 0.08$	$0.98^{0.04}_{0.05}$	$0.97^{0.10}_{0.09}$	$0.022^{0.004}_{0.003}$	$0.14^{0.05}_{0.04}$	$0.62^{0.10}_{0.18}$	$0.40^{0.13}_{0.13}$	$0.05^{0.02}_{0.02}$	$(0.65^{0.08}_{0.08})$	$13.7^{1.6}_{1.6}$
Flat	(1.00)	$0.95^{0.09}_{0.08}$	$0.021^{0.003}_{0.003}$	$0.13^{0.04}_{0.04}$	$(0.57^{0.12}_{0.37})$	$(0.48^{0.24}_{0.24})$	$0.06^{0.02}_{0.02}$	$(0.61^{0.13}_{0.13})$	$14.3^{0.6}_{0.6}$
Flat & LSS	(1.00)	$0.98^{0.10}_{0.07}$	$0.021^{0.003}_{0.003}$	$0.13^{0.01}_{0.01}$	$0.62^{0.07}_{0.07}$	$0.38^{0.07}_{0.07}$	$0.05^{0.01}_{0.01}$	$0.62^{0.06}_{0.06}$	$14.5^{0.7}_{0.7}$
Flat & SN1a	(1.00)	$0.98^{0.11}_{0.09}$	$0.022^{0.003}_{0.003}$	$0.12^{0.01}_{0.02}$	$0.68^{0.04}_{0.06}$	$0.33^{0.05}_{0.05}$	$0.05^{0.01}_{0.01}$	$0.66^{0.05}_{0.05}$	$14.0^{0.6}_{0.6}$
Flat, LSS & SN1a	(1.00)	$1.03^{0.10}_{0.09}$	$0.023^{0.003}_{0.003}$	$0.13^{0.01}_{0.01}$	$0.66^{0.04}_{0.06}$	$0.33^{0.05}_{0.05}$	$0.05^{0.01}_{0.01}$	$0.66^{0.05}_{0.05}$	$14.0^{0.6}_{0.6}$

Table 1: Results of parameter extraction using successively more restrictive priors, following [28]. The confidence intervals reported are at the 1-σ level. The values are reported after marginalizing over all other parameters. All entries have at least a weak prior in which set the prior for all models which do not satisfy $0.45 < h < 0.90$ and age > 10 Gyr to zero. The LSS[11] and SN1a supernovae [24, 29] priors are described in [28]. The stronger h prior is a Gaussian. Parentheses are used to indicate parameters that did not shift more than 1-σ or which depend more on the priors assumed than on the CMB data, in which case the derived range reflects the choice of prior, rather than a constraint by the CMB. The age column is in units of Gyr. See [14].

to plan, MAP, like COBE, will provide us with tools to study cosmogony for years to come. And even there the story does not end, as hosts of new experiments are being designed, commissioned and used to make ever more sensitive measurements, and to open new windows to the early universe such as polarization.

References

[1] Penzias, A.A. & Wilson, R.W., 1965, ApJ, **142**, 419.

[2] Dicke, R. H.; Peebles, P. J. E.; Roll, P. G.; Wilkinson, D. T., 1965, ApJ, **142**, 414.

[3] D.J. Fixsen, E.S. Cheng, J.M. Gales, J.C. Mather, R.A. Shafer, and E.L. Wright, 1996, ApJ, 473, 576

[4] The COBE WWW page, http://space.gsfc.nasa.gov/astro/cobe/cobe_home.html

[5] The RadPack WWW page, http://bubba.ucdavis.edu/~knox/radpack.html

[6] The CMBFast WWW page, http://www.physics.nyu.edu/matiasz/CMBFAST/cmbfast.html

[7] Miller et al., 1999, ApJL, 524:L1.

[8] Torbet et al., 1999, ApJL, 521:L79.

[9] Devlin et al., 1998, ApJL, 509:L69.

[10] Mauskopf et al., 2000, ApJL, 536:L62.

[11] J.R. Bond and A.H. Jaffe, 1999, Phil. Trans. R. Soc. London, 357, 57.

[12] Crill, B.P., 2001, Caltech Ph.D. Thesis.
Available at http://www.physics.ucsb.edu/~boomerang/papers.html.

[13] de Bernardis, P. *et al.*, 2000, *Nature*, **404**, 955–959.

[14] Netterfield, C.B., *et al.*, 2001, Submitted to ApJ. Available at http://www.physics.ucsb.edu/~boomerang/papers.html.

[15] Masi, S. et al., 2001, ApJ, in press.

[16] http://hpcf.nersc.gov.

[17] Borrill, J., 1999, Proc. of the 3K Cosmology ECTMR conference, eds. L. Maiani, F. Melchiorri, N. Vittorio, AIP CP 476, 277.

[18] Hivon, E., Górski, K., Netterfield, B., Crill, B., Prunet, S. and Hansen, F., 2001, ApJ, in press.

[19] Halverson, N.W. et al., 2001, submitted to ApJ.

[20] Leitch, E.M. et al., 2001, submitted to ApJ.

[21] Pyrke, C. et al., 2001, submitted to ApJ.

[22] Hanany, S. et al., 200, ApJ, 545, 5

[23] J.R. Bond and A.H. Jaffe, Phil. Trans. R. Soc. London **357**, 57 (1999), astro-ph/9809043.

[24] Riess et al., 1998, Astron. J. **116**, 1009

[25] S. Perlmutter et al., 1999, Astrophys. J. **517**, 565.

[26] de Bernardis, P. et al. 2001, ApJ, submitted.

[27] Tytler, D. et al., 2000, Phys. Scr., submitted.

[28] Lange, A.E., *et al.*, 2001, Phys. Rev. D, 63, 042001

[29] S. Perlmutter et al., 1999, ApJ, 517, 565

[30] Prunet, S. et al., 200, in "Energy densities in the Universe", Bartlett, J., Dumarchez, J. eds., Editions Frontires, Paris.

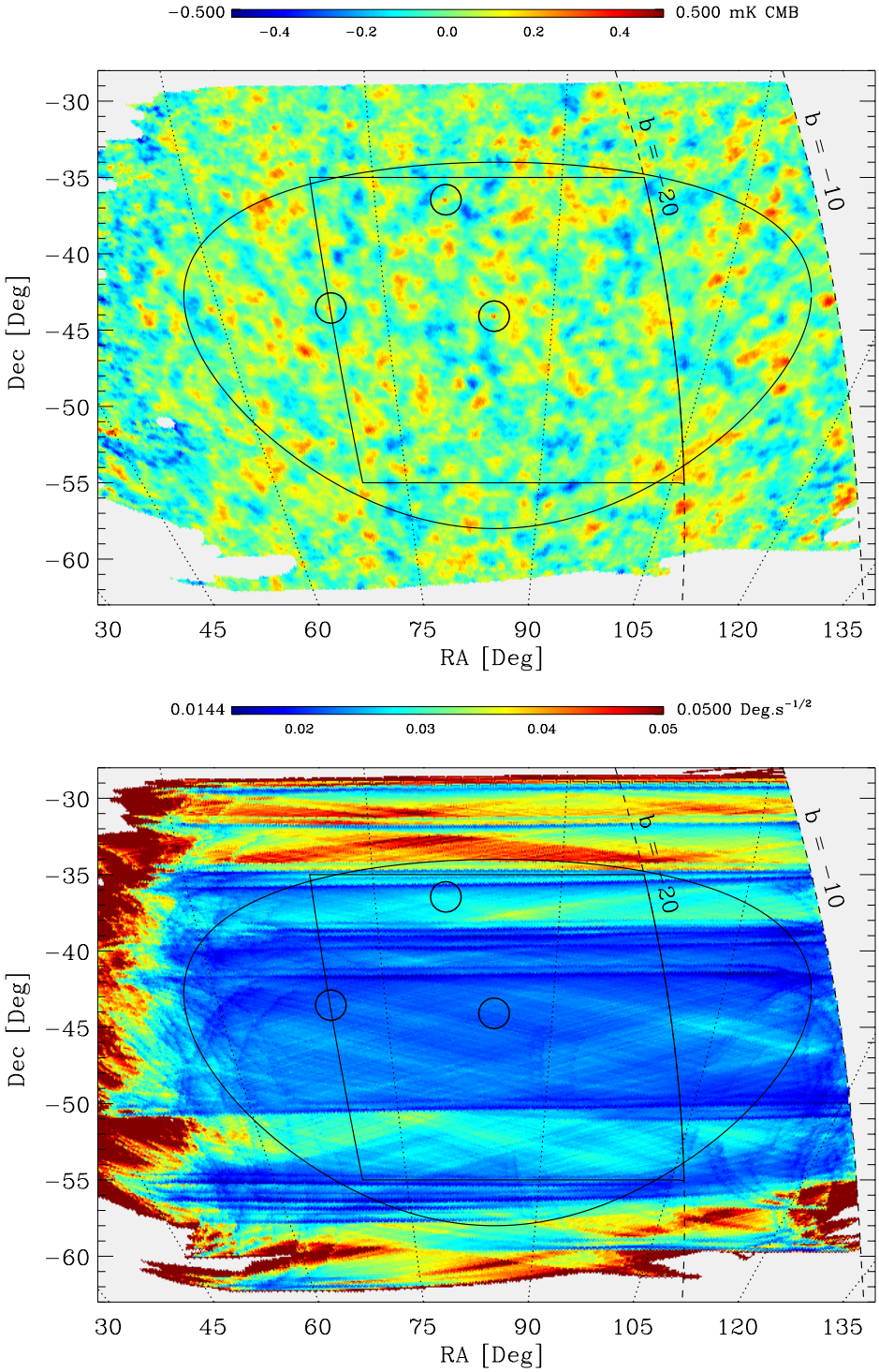

Figure 8: Top panel: BOOMERanG 150 GHz map. The inner rectangle defines the region of sky used in [13]. The larger oval defines the region of sky used in [14]. The three circles indicate brighter radio sources. Bottom panel: A measure of the expected statistical weight as a function of sky coverage. See [14].

PrHEP hep2001

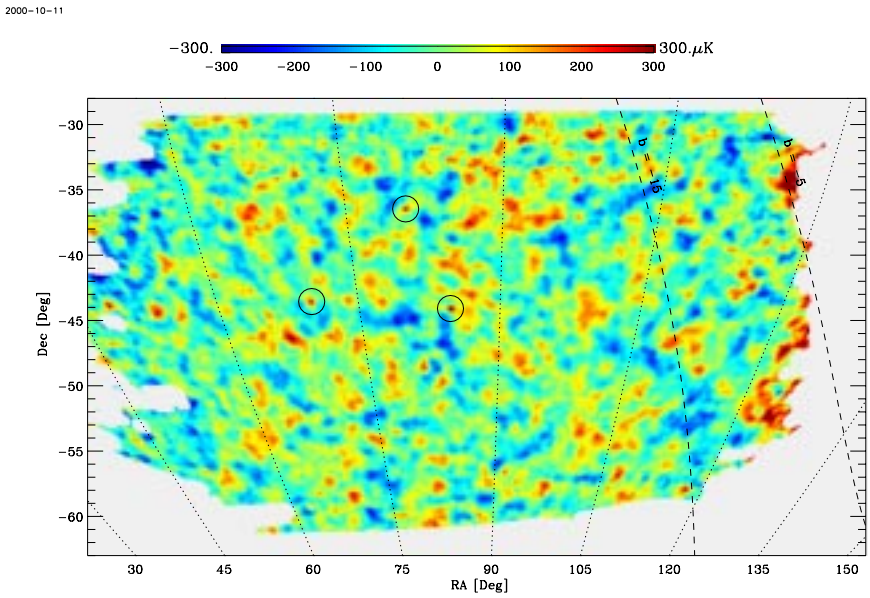

Figure 9: A 90 GHz map. The three extragalactic point sources are circled and are brightest at this frequency. To produce this map, the data have been filtered in the time domain with a filter corresponding to 10 degrees on the sky, so structures which are larger than 10 degrees along the scan direction are not present in the map. The final map has been smoothed with a 20 arc-minute Gaussian filter. See [12].

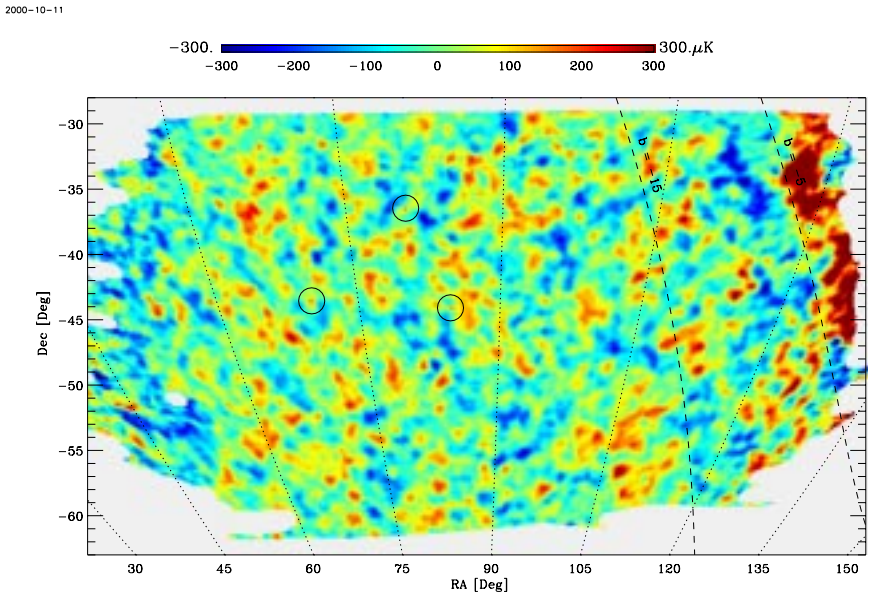

Figure 10: A 150 GHz map. Time domain and spatial filtering is the same as in the 90 GHz map (Figure 9). The galactic signal to the right of the map at b>-5 saturates the color scale, but is confined to the region near the galactic plane. See [12].

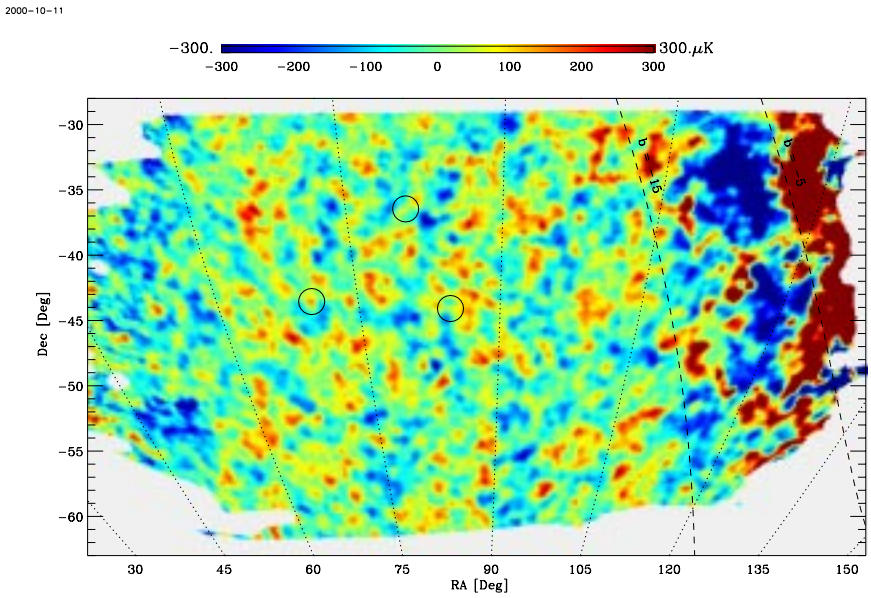

Figure 11: A 240 GHz map. Time domain and spatial filtering is the same as in the 90 GHz map (Figure 9). Note the prominent galactic signal at low galactic latitudes, b>-15. The large gradient at low galactic latitudes is an artifact of the high pass filtering, which sets the average signal at scales larger than 10° equal to zero. See [12].

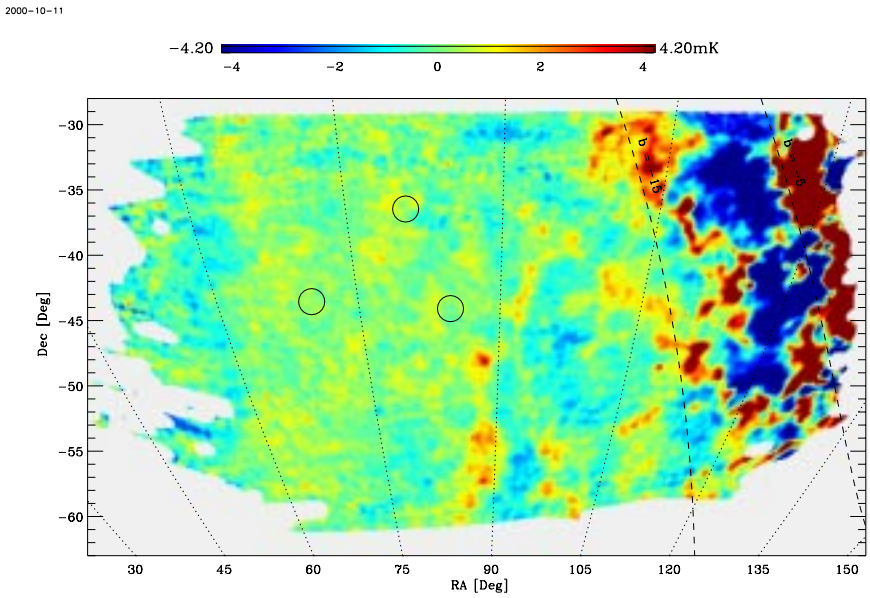

Figure 12: A 400 Ghz map. No degree scale structure is evident. Low galactic latitude signal (b>-15) is correlated with the structure in the 150 GHz and 240 GHz maps (Figures 10 and 11), and galactic cirrus is visible at higher galactic latitude. The time domain and spatial filtering of the 400 GHz data is the same as in the 90 GHz map (Figure 9). See [12].

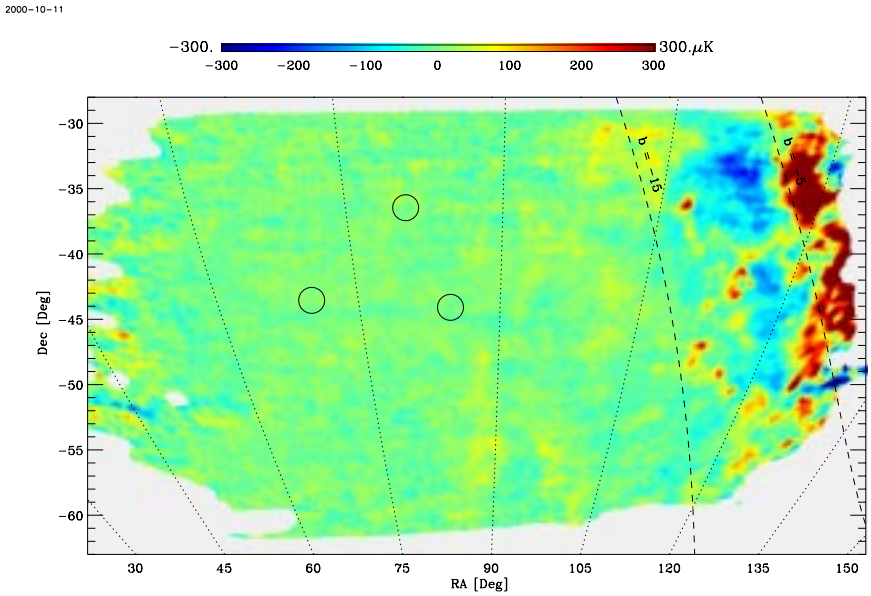

Figure 13: The difference between the proceeding 240 GHz and 150 GHz maps from Figures 10 and 11. No degree scale structure remains, and there is a correlation with the 400 GHz map (Figure 12). See [12].

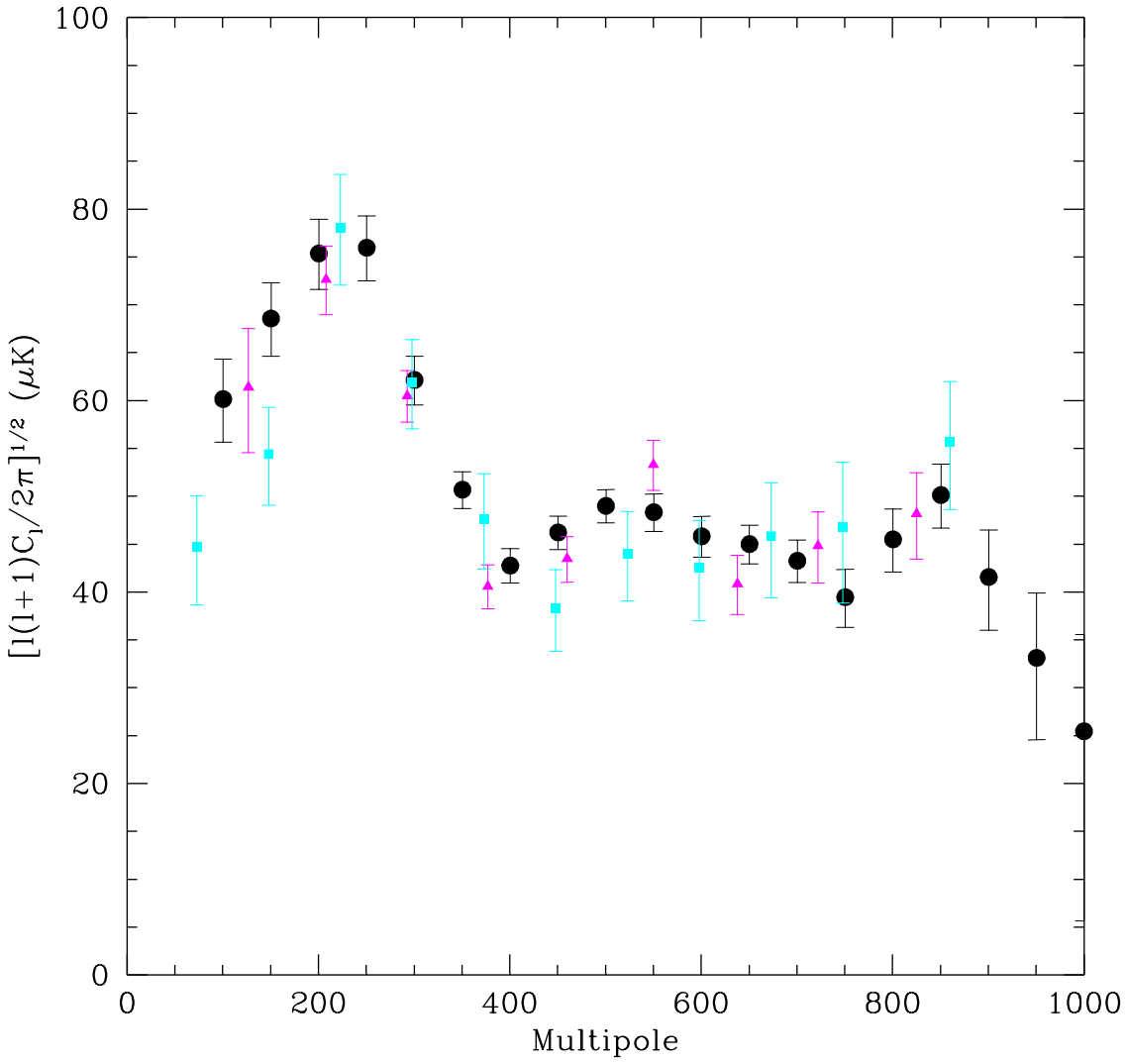

Figure 14: Power Spectra from the BOOMERanG (black), DASI(magenta) and MAXIMA (light blue) experiments.

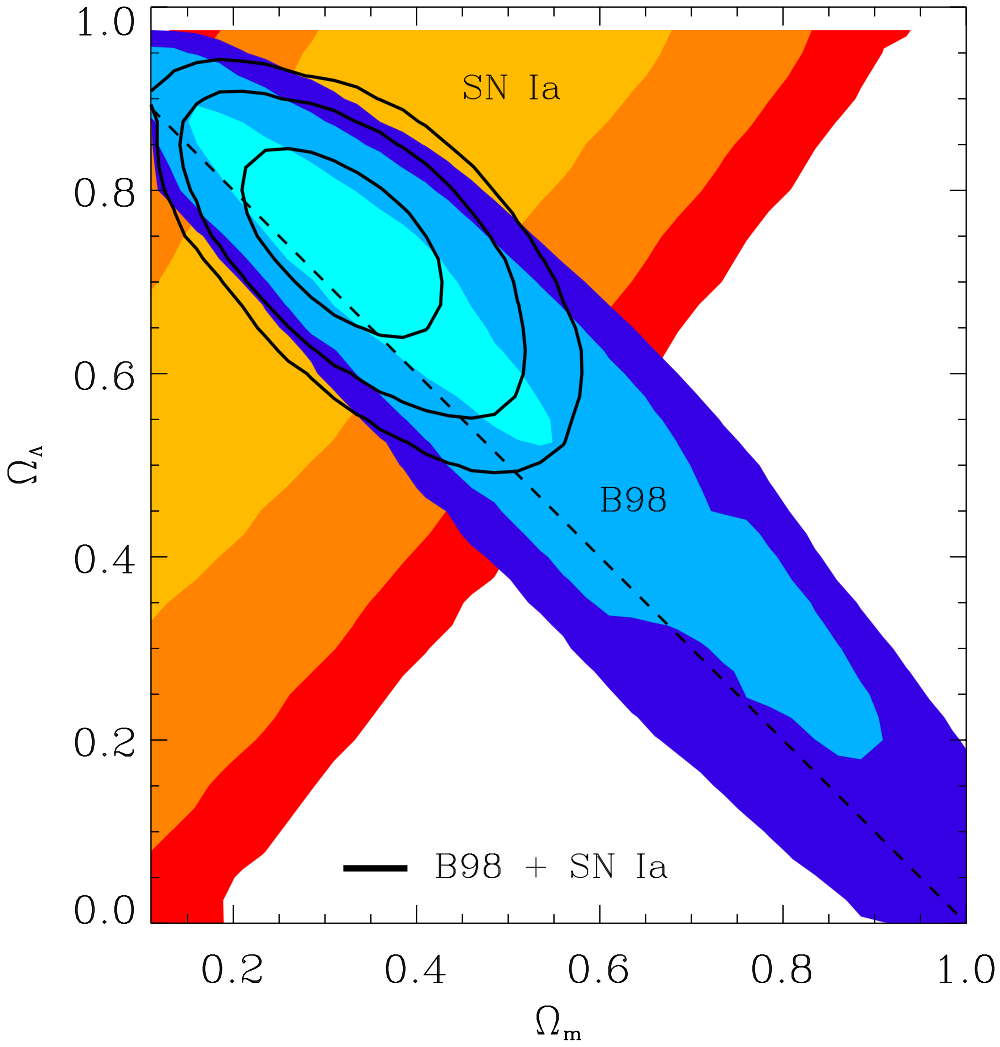

Figure 15: Probability contours in the $\Omega_m\,(=\Omega_c+\Omega_b)/\Omega_\Lambda$ plane. The blue contours are probabilities derived from BOOMERanG showing its power in finding the *total* energy density, but its lack of discriminatory power in differentiating Λ from matter densities. Results from type 1a supernovae are shown in red/orange to demonstrate their complimentarity with CMB measurements. The combination of the two is shown at black line contours. See [26].

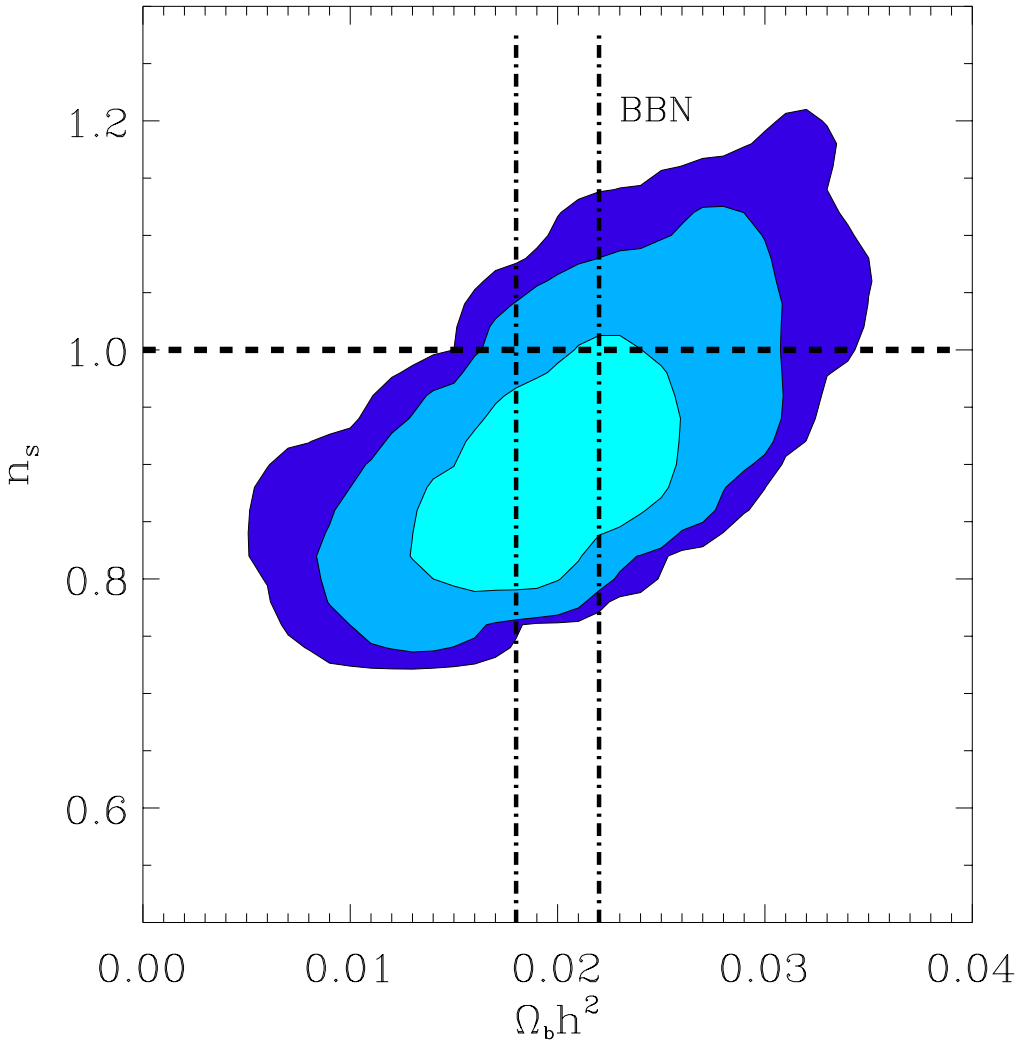

Figure 16: Probability contours in the $\Omega_b h^2/n_s$ plane. The horizontal line indicates a value of $n_s = 1$, indicative of what is often expected in simple inflationary scenarios, while the two vertical lines bracket the limits obtained in [27]. See [26].

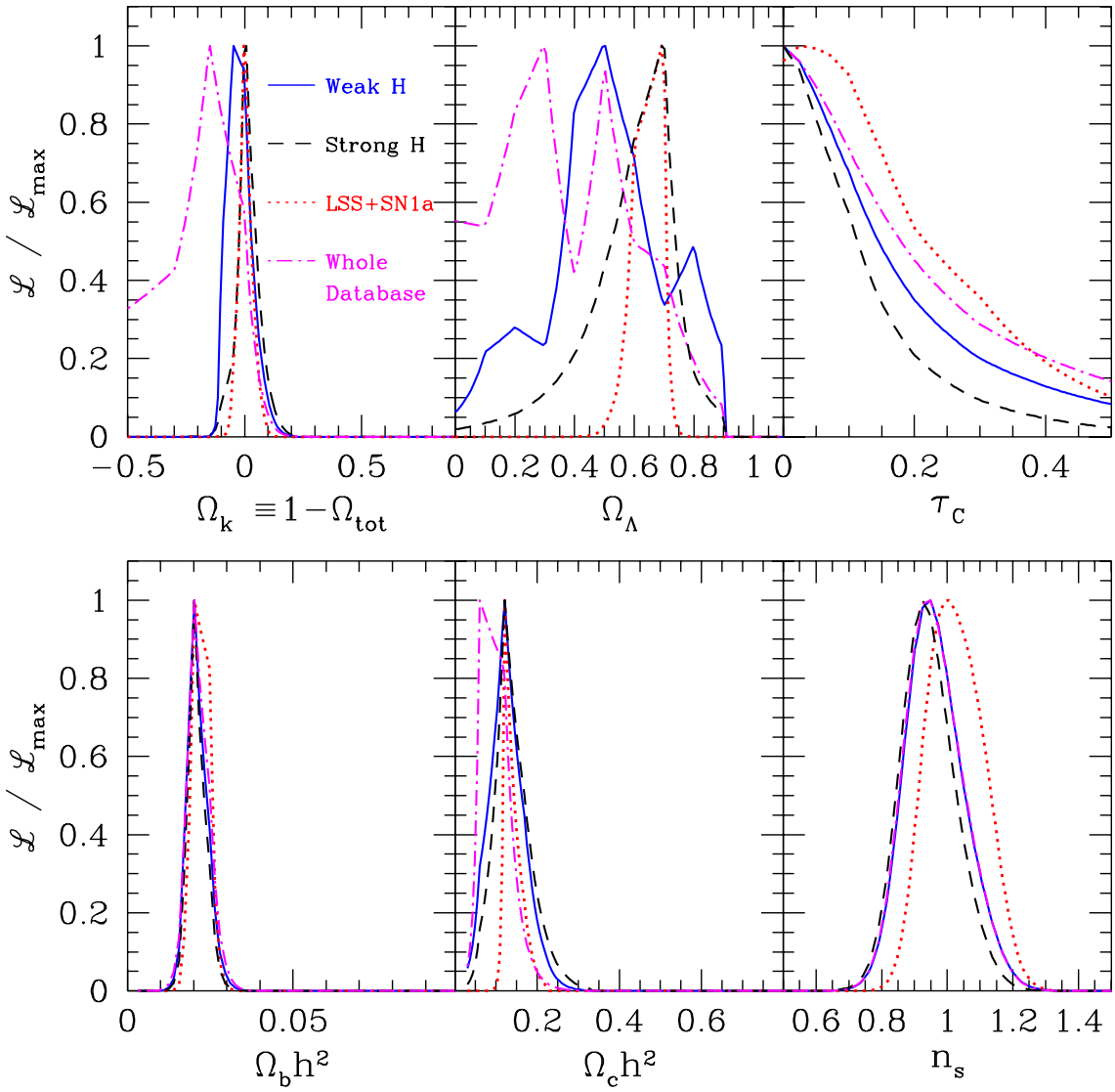

Figure 17: Probability curves obtained by marginalizing over all but the parameters of interest in our hypersurface of probabilities. Each pane has four curves, corresponding to different priors. The curve "weak H" corresponds to the prior which assumes that $0.45 < h < 0.90$. "Strong H" assumes that $0.64 \leq h \leq 0.8$. "LSS+SN1a" assumes $0.45 < h < 0.90$ and adds constraints from Large Scale Structure measurements [23] and from type 1a supernovae measurements [24, 25]. The "whole database" assumes a uniform prior in all models tested, and zero for all others. See [14].